February 23rd, 2023

A Faraday Wave Instability Analog in Vibrated Gas-Fluidized Granular Particles

Qiang Guo[1], Wei Da[1], Ryan Wu[1], Yuxuan Zhang[1], Jingyi Wei[1], Christopher M. Boyce[1*]

[1]Department of Chemical Engineering, Columbia University

(*) Corresponding author. Email: cmb2302@columbia.edu.

Abstract

Granular materials are critical to many natural and industrial processes, yet the chaotic flow behavior makes granular dynamics difficult to understand, model and control, causing difficulties for natural disaster mitigation as well as scale-up and optimization of industrial devices. Hydrodynamic instabilities in externally excited grains often resemble those in fluids, but have different underlying mechanisms, and these instabilities provide a pathway to understand geological flow patterns and control granular flows in industry. Granular particles subject to vibration have been shown to exhibit Faraday waves analogous to those in fluids; however, waves can only form at high vibration strengths and in shallow layers. Here, we demonstrate that combined gas flow and vibration induces granular waves without these limitations to enable structured, controllable granular flows at larger scale with lower energy consumption for potential industrial processes. Continuum simulations reveal that drag force under gas flow creates more coordinated particle motions to allow waves in taller layers as seen in liquids, bridging the gap between waves produced in conventional fluids and granular particles subject to vibration alone.

I. INTRODUCTION

Granular materials, such as sand or catalytic particles, are ubiquitous in nature and industry [1], and the complexity of granular flows continues to confound physicists, geoscientists, applied mathematicians and engineers. However, the importance of granular flows in understanding natural phenomena [2] from mudslides to volcanos and developing new technologies [3] in areas ranging from carbon capture to sustainable mining keeps researchers from a wide range of fields searching for ways to model and control these flows. Grains subject to external forcing, e.g. shear [4], vibration [5], or gas flow [6], can display remarkable similarities to fluid flows [7,8]. In particular, granular materials have been demonstrated to undergo flow instabilities analogous to those in liquids, such as gas bubbling [5,6], shear-induced waves [4], Rayleigh-Taylor fingering [8–10] and Rayleigh-Bénard convection [8,11], often with mechanisms different from those in conventional fluids. Such instabilities present ideal systems for investigating the commonalities and differences between the physics governing liquid and granular flows, as well as challenging phenomenological and rheological models for granular flows [12–14]. The structured nature of many of these flows creates an opportunity to improve agricultural and industrial processes involving granular flows because device design and optimization are often hampered by mathematically chaotic motion [15,16] and unpredictable scale-up [17].

Faraday waves are a type of parametric waves which occur in Newtonian fluids subject to vertical vibration [18]. Analogous waves have been observed in vibrating shallow granular layers with a few mm tall [19] ($H \sim 10\ d_p$, where H is the layer height and d_p is the particle diameter), forming patterns of oscillons [20], squares, stripes, hexagons and flat layers with kinks [21]. The pattern formed in granular materials is determined largely by the dimensionless vibration strength ($\Gamma = \frac{4\pi^2 A f^2}{g}$, where A and f are the driving amplitude and frequency and g is gravitational acceleration) and the dimensionless driving frequency ($f^* = f\sqrt{\frac{H}{g}}$) [21,22]. The mechanism for pattern formation is distinct from that in fluids since (i) the granular layer leaves the bottom plate when $\Gamma > 1$ due to a lack of surface tension between granular particles and surrounding gas, making the pattern formation dictated by time scales for the layer free flight and particle mobility and (ii) layer height is a small multiple of the particle diameter, making d_p play a role in mobility and pattern formation [23]. Despite the wide scientific interest surrounding parametric waves in vibrated granular particles, the industrial applicability appears limited since most patterns have been demonstrated only in shallow layers, patterns only form above $\Gamma \sim 2.5$ and most studies have been conducted in gas-evacuated containers [21].

Pulsed gas flow [24,25] can also form parametric waves in granular materials. The onset of patterns [24] is dictated by f_{gs}^{*} (with f_{gs} the frequency of gas flow pulsation) and $\Gamma_{\mathrm{gs}} = \frac{u_a}{u_t \overline{\phi}}$, where u_a is the amplitude of gas velocity oscillations, u_t is the terminal velocity of the particles in the gas and $\overline{\phi}$ is the average solids volume fraction. The strong effect of drag force on the formation of these patterns further suggests that the mechanism for pattern formation is significantly different from that due to vibration [24]. The potential to apply pulsed gas flow to industrial processes is complicated by the fact that bubble formation destroys structure at higher gas driving strengths and non-shallow layer heights [26].

Subjecting granular particles to combined upward gas flow and vibration can induce fluid-like motion in granular materials with strong attractive forces [27] as well as suppress bubble formation and create a regime in which particles move yet no bubbles are present [10]. In this regime, particles have been shown to exhibit structured flow instabilities analogous to Rayleigh-Taylor fingering [10] and Rayleigh-Bénard convection [11].

Herein, we demonstrate that combined constant gas flow and vibration can induce Faraday wave analogs in granular layers. These waves persist in layers over an order of magnitude taller than those achieved by prior works which used either only vibration or pulsed gas flow [19,25,26,28]. The onset of patterns occurs at Γ significantly lower than those in vibrated containers, including $\Gamma < 1$ in some cases. These features for wavy patterns address the issues of (i) chaotic motion and (ii) unpredictable scale-up in gas-fluidized granular particles as well as the issues of (a) short layer heights and (b) strong vibration strengths in vibrated granular Faraday waves. Thus, these features create desirable dynamics for industrial granular flows. We capture the effect of gas flow on the onset of waves by incorporating constant gas velocity and vibrating plate velocity into a dimensionless velocity, collapsing data across different gas velocities and particle properties. A continuum particle model coupled with a gas flow model can capture the waves, showing how drag from gas flow increases the uniformity of vertical forces on particles throughout the layer, explaining differences between waves formed in granular particles with and without gas flow. The fluid-like nature and pattern formation in tall layers enabled by drag makes these waves analogous to Faraday waves in conventional fluids [29], yet the lack of surface tension and layer leaving contact with the bottom plate makes the waves analogous to those in granular particles subject to vibration alone. As such, the waves reported in this article provide a bridge and impetus to study Faraday waves in a wider range of complex fluids.

II. METHODS

A. Experimental setups

A pseudo-2D and a 3D cylindrical fluidized bed were used in separate experiments. The pseudo-2D fluidized bed had a width of 200 mm, a depth of 10 mm and a height of 500 mm. The 3D cylindrical fluidized bed had an inner diameter of 178 mm and a height of 500 mm. Both beds were made of polymethyl methacrylate. **Fig. S1** [30] schematically illustrates the experimental setups.

Air at ambient conditions was first bubbled through a humidifier to minimize electrostatic forces built on granular particles and then passed through a wind box and a 3 mm-thick sintered bronze distributor plate with an average pore size of 15 μm that is fixed between two polymethyl methacrylate sheets before entering the bed of particles. Even distribution of gas at the bottom was ensured due to the thickness and pore size of the sintered bronze distributor plate. The gas flow rate was precisely controlled using a mass flow controller (Alicat, MCP series with a full range of 10, 50, or 250 slpm).

To add vibration, the fluidized bed was placed on top of an electrodynamic shaker (Labworks Inc., ET-140), which generated a vertical sinusoidal displacement, $\delta = A\sin(2\pi f t)$, where t is the time, using a controller (Labworks Inc. VL-144), an amplifier (Labworks Inc., PA-141) and an accelerometer (PCB Piezotronics Inc., J352C33).

A high-speed camera (AOS Technologies, PROMON U750) was used to record the bed behavior. The light illumination and camera arrangements were different between the pseudo-2D and 3D fluidized beds. For the pseudo-2D bed, a LED light was placed behind the bed and the camera was placed in front of the bed, such that particles are displayed in black and gas voids and bubbles are displayed in white in the recorded images. With such a protocol, we cannot image patterns with a layer height lower than 25 mm because they are hidden by the upper polymethyl methacrylate sheet that is used to fix the distributor plate. For the 3D cylindrical bed, three LED lights were placed around the bed and the camera was placed above the bed, focusing on the bed surface. For all experiments, images were taken at a frame rate of 100 frames per second.

Spherical particles were used with the density and size specifications given in the figures and tables as quoted by the manufacturer. Glass beads and ceramic beads were ordered from Ceroglass Technologies Inc. Silica-alumina beads were ordered from Sigma-Aldrich.

B. Identification of regime map and onset vibration strength

The following procedures were followed to create the regime map for different patterns and to obtain the onset of vibration strength for pattern formation. At first, a certain amount of particles was added to the system to reach a target layer height. The layer height was measured after a fluidization-defluidization process. Then, the gas flow rate was tuned to a value at 1.5 U_{mf}. Here, U_{mf} is the minimum gas velocity needed to suspend the particles without vibration, due to drag force on particles overcoming gravity. The U_{mf} values of different particles were determined by slowly decreasing the gas velocity from a bubbling state until no bubbles or particle motion were observed. Note that U_{mf} decreases by adding vibration [31], but for consistency we always refer to U_{mf} without vibration. For the regime map experiments, after a steady state was reached, vibration with a frequency of 30 Hz was turned on. At this vibration frequency, the vibration strength was programmed to be log-linearly decreased (the typical speed is to decrease the vibration strength from 3 to 0.5 in 400 s). During this process, the critical vibration strength for the transition between two patterns and the lowest vibration strength below which the pattern was not formed were identified. Subsequently, the vibration frequency was decreased and at a set vibration frequency, the vibration strength was again decreased to identify the critical vibration strength. This process was continued until reaching a vibration frequency of 2 Hz. Similarly, the gas flow rate was decreased until reaching a gas flow rate of 0 and at a set flow rate, the vibration frequency was decreased in stages from 30 Hz to 2 Hz.

C. Continuum modeling simulations

Two-fluid modeling (TFM) [32] was used to model gas and particles as interpenetrating continua coupled by a drag law [33], while utilizing complex rheology to model the ensemble of particles as a continuous fluid. MFiX [34], an open-source software developed by the National Energy Technology Laboratory was used. Both a pseudo-2D and a 3D fluidized bed were simulated. **Table S1** [30] lists the detailed parameters used in simulations.

The simulated pseudo-2D system had a width of 200 mm, a depth of 2 mm, and a height of 120 mm. The simulated 3D system had a width and depth of 100 mm and a height of 45 mm. In both the pseudo-2D and 3D TFM simulations, the modeled gas phase had a viscosity of 1.8×10^{-5} Pa·s and a density of 1.2 kg/m^3, similar to the properties of air at atmospheric pressure. The modeled particulate phase had a size of 250 μm and density of 2500 kg/m^3, similar to the glass beads used in experiments with a size of 200-300 μm and a density of 2500 kg/m^3. Initially, the solids phase with a volume fraction of 0.55 was loaded into the bed at a layer height of 5, 10, 15, 20, 30, or 60 mm for the pseudo-2D simulations and 6 mm or 10 mm for the 3D simulations. The grid size was 1 mm (horizontal) by 1 mm (depth) by 1 mm (vertical), equaling 4 particle diameters in side length. Three scenarios, including combining both gas flow and vibration, vibration only, and pulsed gas flow only, were modeled. Instead of physically moving the bottom plate, vibration was modeled by oscillating the gravitational force following $g = 4\pi^2 f^2 A sin(2\pi f t) - 9.81$. The vibration or pulsed gas flow frequency was 10 Hz. The vibration amplitude used was 3 mm and 4.5 mm for the scenario with combining both gas flow and vibration and the scenario with vibration only, respectively, in the 3D simulations. For the pseudo-2D simulations, the vibration amplitude used was 2 mm for the scenario with combining both gas flow and vibration. The inlet boundary condition was set to a constant superficial gas velocity with $1.1U_{mf}$ and 0 for the scenario with combining both gas flow and vibration and the scenario with vibration only, respectively. For the scenario of pulsed gas flow only, the inlet boundary condition was set to a velocity oscillating with time following Francia et al. [26]: $U/U_{mf} = 1.0+2.0(1+\sin(2\pi 10t))$. The outlet boundary condition was constant atmospheric pressure. The sides of the system were treated as periodical boundaries. The interaction of the gas phase and the solids phase was coupled using the Gidaspow drag law [32]. The kinetic theory of granular flows by Lun et al. [35] was used to close the solids stress due to kinetic contributions, and a recently developed model by Guo et al. [12] was used to close the solids stress due to frictional contributions.

III. RESULTS

A. Experimental Faraday wave patterns

Both a pseudo-2D and a 3D cylindrical container of granular particles were subjected to constant upward gas flow while placed on top of an electrodynamic shaker to induce vertical vibration (**Fig. S1** [30]). Wavy patterns persist to tall layer heights in pseudo-2D systems without notable changes in wavelength and amplitude of the patterns (**Fig. 1a**, **Video S1** [30]). The waves repeat their dynamics every two vibration cycles (**Fig. 1b**) and decrease in wavelength and amplitude with increasing driving frequency (**Fig. 1c**), indicating that they are analogous to Faraday waves. As with waves formed in 3D ensembles of grains subject to vibration alone [20,21], granular particles subject to combined vibration and constant gas flow exhibit oscillons, squares, stripes, hexagons and flat layers with kinks (**Fig. 1d**) and this progression of patterns tends to arise as Γ and f are increased. Further, the wavelength of 3D waves decreases with increasing driving frequency (**Fig. 1e, f**), while increasing with increasing layer height (**Fig. 1g**).

Wavy patterns persist in granular layers up to $H \sim 100$ mm and ~1250 d_p in pseudo-2D systems and up to $H \sim 130$ mm and ~520 d_p in 3D systems (**Table S2**, **Video S1**, **Fig. S2** [30]). Degradation above this height was due in part to (i) the wavelength of waves reaching the bed diameter, (ii) the power of the shaker not being able to handle the weight of the particles and (iii) the emergence of bubbles in system. Since stronger vibration has been shown to suppress bubbling [10], we expect waves could persist to even higher layer heights if a larger system and a stronger shaker were used. The persistence of waves is significantly higher in H/d_p than the highest found values in prior work: ~26× [19] and 16× [28] than vibration alone in 3D and 2D, respectively, and 6.5× [25] and 43× [26] pulsed gas flow in 3D and 2D, respectively (**Table S2** [30]). Upward gas flow, not just interstitial gas, is critical to waves persisting to higher H/d_p because with vibration only and atmospheric air, 3D experiments did not produce waves at $H/d_p > 24$ (**Fig. S3** [30]).

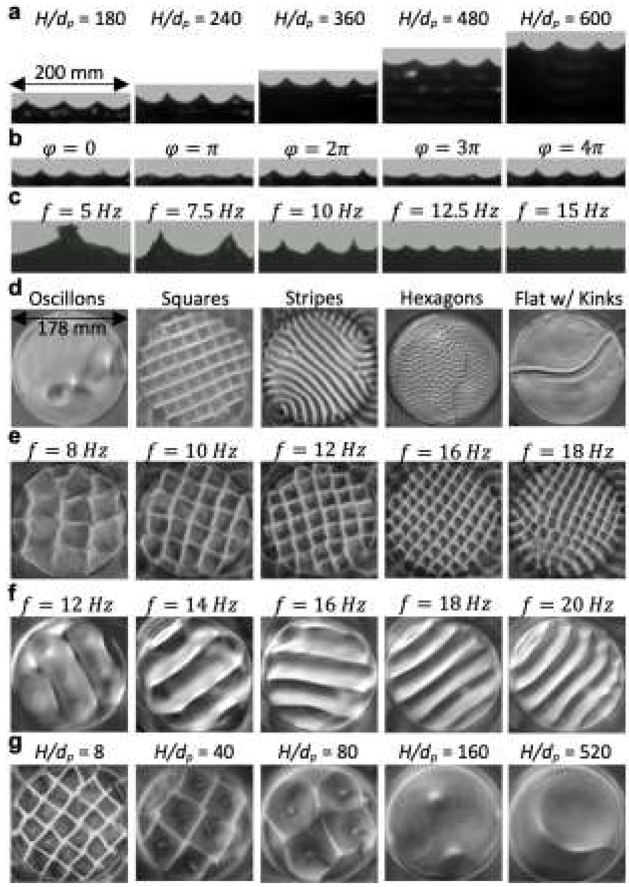

Fig. 1 Images of Faraday waves in granular particles in a pseudo-2D system (a-c): (a) the effect of H on waves, (b) the periodic repetition of the waves at $f/2$, (c) the effect of f on waves. (d) Shows different waves patterns formed in a 3D system, (e) and (f) show the effect of f on 3D wavelength with (e) showing the square patterns and (f) showing the stripe patterns, (g) shows 3D waves at different H. Particles: (a-b) glass beads with d_p = 200-300 μm and ρ_p = 2500 kg/m^3; (c) silica-alumina beads with d_p = 53-106 μm and ρ_p = 1530 kg/m^3; (d-g) ceramic beads with d_p = 200-300 μm and ρ_p = 6060 kg/m^3.

B. Regime maps and onset of Faraday wave patterns

Without gas flow, Faraday wave patterns only form at $\Gamma > 2.5$, if at all (**Fig. 2**). When constant gas flow is applied, wave patterns form at significantly lower Γ, less than one in some cases, and a wide range of patterns are observed, including multiple patterns observed simultaneously (**Fig. 2**). While prior studies for vibration alone have collapsed pattern formation results using Γ and f^* [21,22], **Fig. 2** shows that when constant gas flow is applied, the patterns formed also depend on H as well as the normalized gas velocity, U/U_{mf}. Similar regime maps to those in **Fig. 2** were observed when using particles of different size and density, indicating that different particle properties can be accounted for mostly in their effects on U_{mf}.

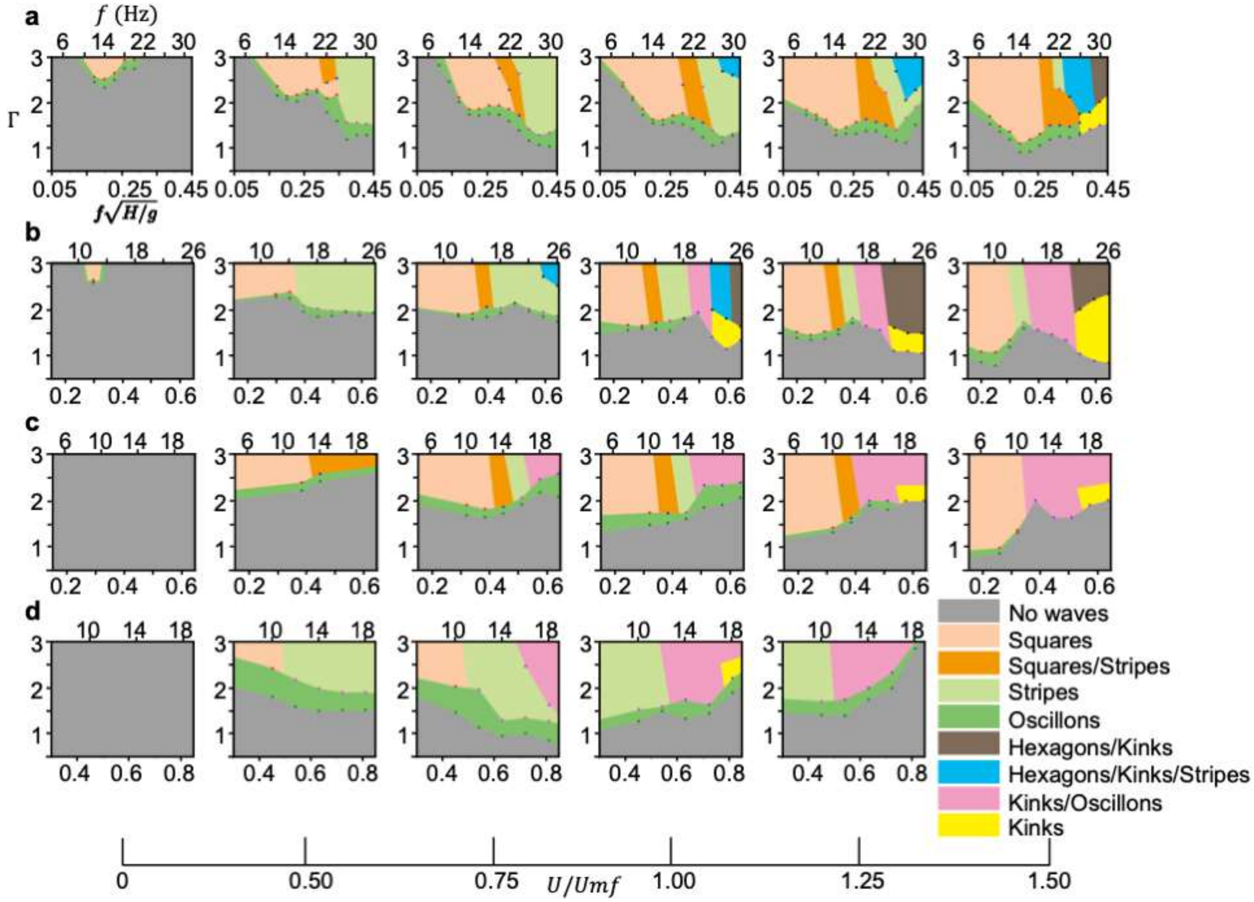

Fig. 2 Regime maps of Γ vs. f^* showing different wave patterns formed in a 3D bed for different H/d_p: (a) 8, (b) 24, (c) 40, and (d) 80 as well as different U/U_{mf} (different columns). Particles: ceramic beads with d_p = 200-300 μm and ρ_p = 6060 kg/m^3.

The decrease in Γ needed to induce the onset of wavy patterns with increasing gas velocity can be observed more directly in **Fig. 3a**. We introduce a parameter $u_{tot}^* = (2\pi Af + U - U_{mf})/U_{mf}$ to create the best collapse of the data for the onset of patterns across a range of gas velocities, vibration amplitudes and vibration frequencies (**Fig. 3b**). u_{tot}^* was obtained by combining the peak velocity of the container and excess gas velocity (difference in gas velocity and U_{mf}), and then normalizing this velocity by U_{mf}. As such, u_{tot}^* combines the effect of gas velocity to induce particles to form a fluid-like state and the peak container velocity causing particles to detach from the bottom plate and subsequently collide with the bottom plate, forming waves. Other potential dimensionless parameters combining gas flow and vibration from the perspective of velocity and acceleration were also tested (**Fig. S4** [30,36]); however, u_{tot}^* proved most effective at collapsing the data and has a clear physical meaning. Here, gas flow and Γ were decreased to find the onset of waves because such an experimental protocol gave the most repeatable results. A slight hysteresis of the critical Γ for pattern formation exists while increasing and decreasing either gas flow or vibration (**Fig. S5** [30]), and more specifically, a slightly larger Γ is necessary to induce the patterns while increasing gas flow rate or Γ.

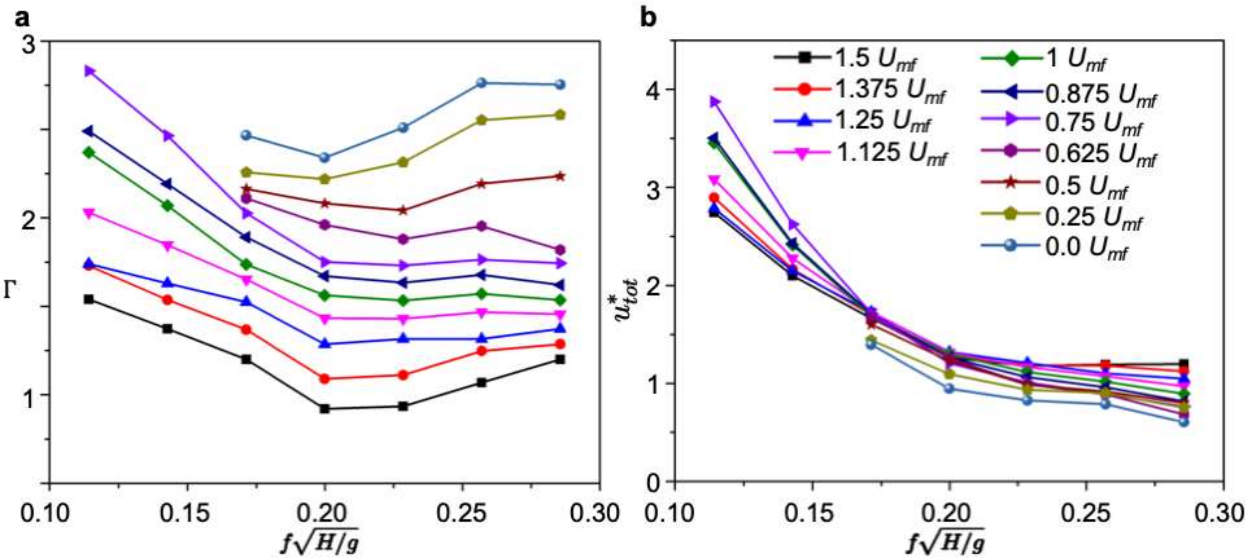

Fig. 3 Onset of Faraday waves in a 3D system for different gas velocities based on $f^* = f\sqrt{H/g}$ and (a) Γ and (b) $u_{tot}^* = (2\pi A f + U - U_{mf})/U_{mf}$. Particles: ceramic beads with d_p = 200-300 μm and ρ_p = 6060 kg/m^3. H = 2 mm.

C. Change of wavelength vs. layer height and vibration frequency

The wavelength of waves formed was directly proportional to the inverse of the vibration frequency squared, f^{-2}, across a range of container, particle, vibration and gas flow conditions (**Fig. 4a**), consistent with prior results for Faraday waves in liquids and granular particles [19,23]. Based on the linear regressions through **Fig. 4a**, an effective minimum wavelength at infinite driving frequency (λ_{min}) and the effective gravity (g_{eff}) can be calculated analogously to the dispersion relationship for gravity waves in a conventional fluid [19] $\lambda = \lambda_{min} + g_{eff}/f^2$. **Table 1** shows λ_{min} and g_{eff} values for a variety of conditions. The g_{eff} value of ~2.7 m/s^2 for square patterns obtained here is similar to that for squares in grains subject to vibration [19], ~3.1 m/s^2. This difference can be explained by drag force from gas flow suspending the particles in a more fluid-like state, giving particles more mobility to move farther in each vibration cycle, creating patterns with longer wavelengths. The larger g_{eff} values for stripes (~7.7 m/s^2) and 2D waves (~5.5 m/s^2) is attributed to a lower mobility in the particles, since they only move in one lateral direction, rather than two in the case of squares. λ_{min} increases with increasing particle size in 3D systems at the same H/d_p, which has been observed previously and attributed to the effect of particle size on energy dissipation [19]. In contrast, λ_{min} does not vary significantly with particle size in pseudo-2D systems, indicating that wall effects dominate energy dissipation in these systems.

Table 1. Wave patterns, minimum wavelength, λ_{min}, and effective acceleration, g_{eff}, based on linear regressions in **Fig. 4a**.

Symbols in **Fig. 4a**	2D /3D	Particle Density (ρ_p, kg/m^3)	Particle Size (d_p, µm)	Layer Height (H, mm)	H/d_p	Pattern	λ_{min} (mm)	g_{eff} (m/s^2)
■	3D	6060	200-300	2	8	Squares	7.97	2.78
●	3D	2500	200-300	2	8	Squares	7.81	2.76
▲	3D	2500	90-150	2	17	Squares	6.75	2.81
▼	3D	2500	90-150	1	8	Squares	3.75	2.47
◀	3D	6060	200-300	15	60	Stripes	10.4	7.72
⬒	2D	6060	200-300	30	120	2D Waves	6.92	5.44
⬒	2D	2500	200-300	30	120	2D Waves	7.35	5.55
⬒	2D	2500	90-150	30	250	2D Waves	6.64	5.53
⬒	2D	2500	200-300	60	240	2D Waves	7.34	5.25

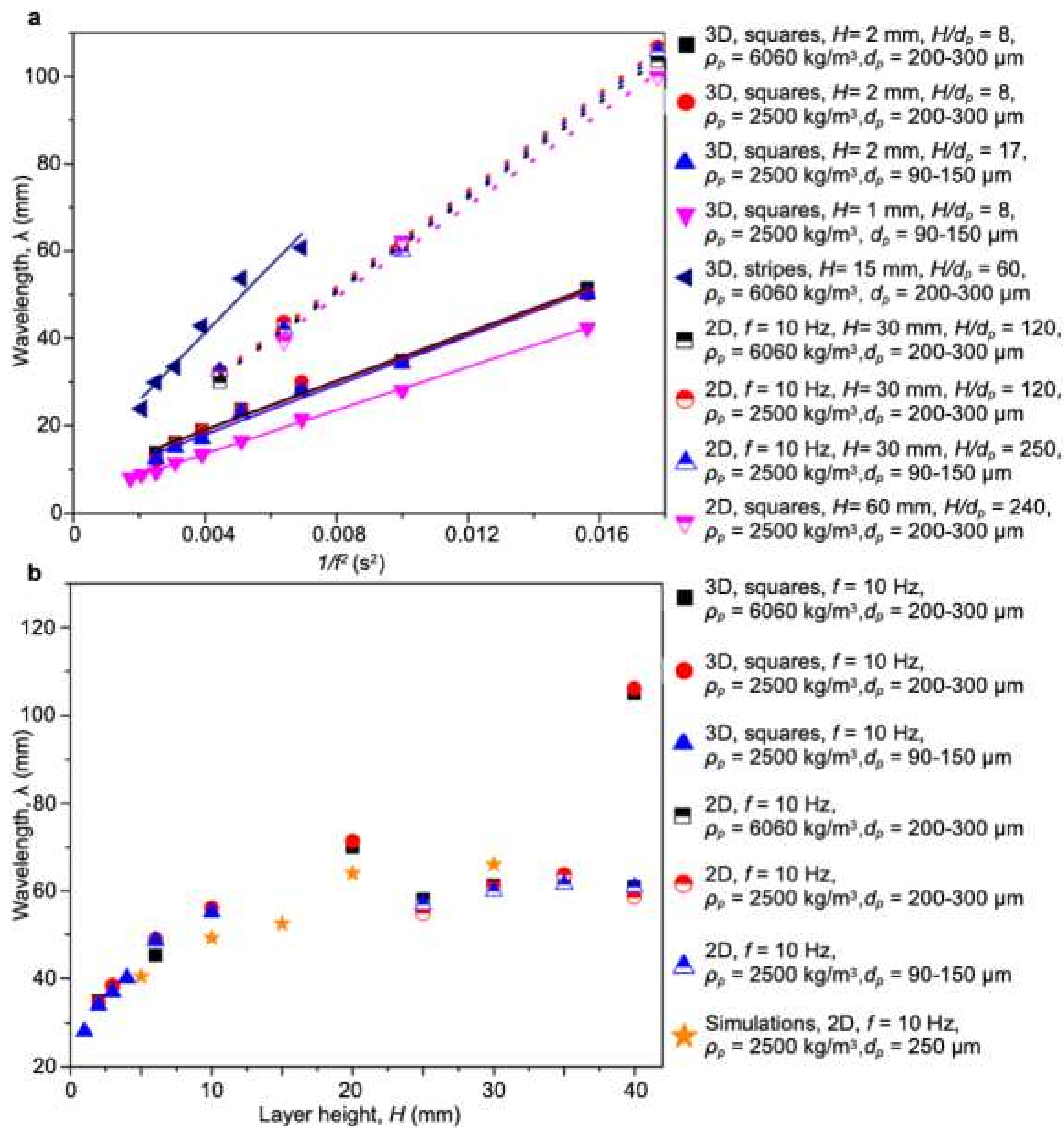

Fig. 4 (a) Wavelength vs. f^{-2} and (b) wavelength vs. H for pseudo-2D and 3D systems with different patterns formed, different layer heights and different particle properties. Lines in (a) show linear regressions through the data.

The wavelength increases with layer height up to the highest height tested in a 3D system (H = 130 mm, H/d_p = 520). We did not test higher heights because, above this height, the wave patterns became influenced by the side walls. For a pseudo-2D system, the wavelength first increases with layer height and then levels off at $H/d_p \sim 80$ (**Fig. 4b**). In contrast, particles subject to vibration alone have been shown to have wavelength level off with increasing layer height above

$H/d_p \sim 7$ [19]. This difference between 3D systems vs. 2D systems can be explained by the added mobility enabled by the fully 3D motion of particles. We attribute the difference in 3D systems with vs. without gas flow to the added mobility created by suspending the particles in a fluid-like state using gas flow. With more particle mobility, as particle layer height is increased, more particles are available to move quickly laterally each vibration cycle, creating longer wavelengths of patterns formed. Note that, due to system geometry in experiments, we were not able to optically visualize pseudo-2D systems with $H < 25$ mm, and thus we have included pseudo-2D simulations (**Fig. S6** [30]) in **Fig. 4b** to show wavelength trends for smaller layer heights.

D. Mechanisms uncovered by continuum modeling simulations

Prior experimental studies for vibration alone have explained that pattern formation occurs due to (1) free flying particles above a vibrating plate colliding with the plate and having vertical momentum differences translate to horizontal motion of particles and (2) particles re-entering free flight for long enough to translate horizontally for waves to form [19]. Prior work suggested that patterns could not form in particle layers with heights above ~10 d_p without significantly increasing Γ because (a) the free flight time of particles at the layer surface becomes too small and (b) the timing of particles colliding with the bottom of the system becomes too spread out to induce coherent motion of particles in waves [19]. Notably, our experiments show that for combined constant gas flow and vibration (i) waves persist in layer heights up to ~520 d_p (**Fig. 1g**) and (ii) Γ needed to produce waves does not change significantly with layer height (**Fig. 2**).

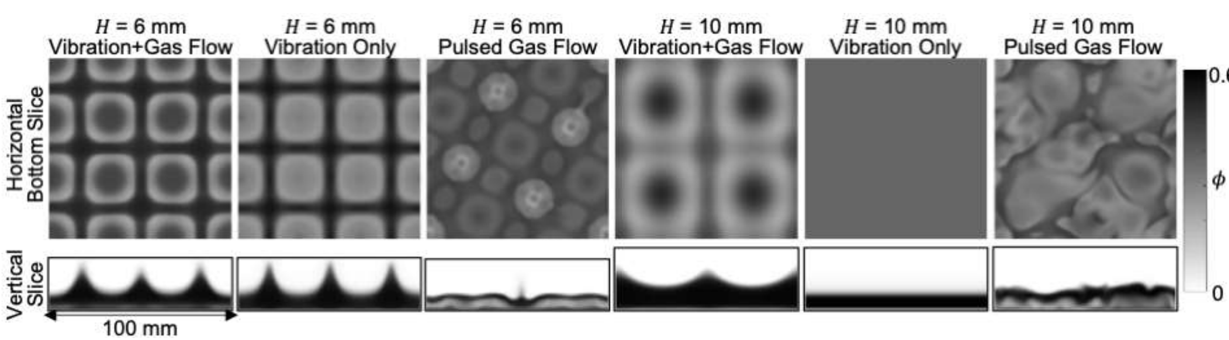

Fig. 5 Continuum simulation results of patterns formed in grains with different layer heights (H/d_p = 24 and 40) under constant gas flow conditions (U/U_{mf} = 1.1) with Γ = 1.2, no gas flow with Γ = 1.8, and pulsed gas flow conditions [26]. Particles: d_p = 250 μm and ρ_p = 2500 kg/m^3.

To examine the physical origins of the differences between Faraday waves in grains subject to constant gas flow and vibration versus vibration alone, we utilize TFM computer simulations. The rheological model recently developed by Guo et al. [12] was used, since it was shown to capture structured bubble dynamics in vibrated gas-fluidized beds by accounting for transitions between fluid- and solid-like behavior in granular particles. This rheological model predicted the Faraday wave patterns formed in grains subject to combined constant gas flow and vibration, vibration alone, or pulsed gas flow (**Fig. 5, Fig. S7** [30]), while other commonly used rheological models [37,38] could not. Simulations show that at low H, waves form in all the three excitation techniques, yet cases with vibration alone require a larger Γ to produce waves, matching experimental results (**Fig. 2**). Further, waves continue to form at higher H for combined vibration and constant gas flow, yet waves do not form with vibration alone, as seen experimentally in **Fig. S3** [30]. Simulations also show that, when pulsed gas flow is used, bubble formation interferes with waves forming at the taller layer height. Further, as compared to cases involving vibration, the minimal solids volume fraction in the horizontal bottom slice is much higher and the solids volume fraction oscillation is out-of-phase (**Fig. S8** [30]), indicating a difference in mechanism between cases involving pulsed gas flow vs. vibration.

Fig. 6 shows a time series of simulation results spanning between two subsequent moments of particle impact with the bottom plate (as shown from the solids pressure) to demonstrate why waves continue to form at tall layer heights when constant gas flow is used, yet waves do not form without gas flow. In both cases, high solids pressure sets in when the particles are in contact with the bottom plate, and solids pressure becomes close to zero when particles are in free flight. For the case with gas flow, particles are moving downward relative to the plate when they collide, but the particles have little horizontal velocity, and drag force acts upward on particles, dampening their landing. Collision causes the particles to move upward quickly relative to the plate, and some vertical momentum change is shifted into horizontal momentum, driving particles to move away from crests towards troughs in the waves. As such, when particles are in free flight, crests and troughs invert. For the case with no gas flow, the relative velocity between the particles and plate as well as the drag force vary with vertical position of particles in the layer, indicating that particles experience vastly different motion and forces based on their position in this deep layer. As such, particle collision with the bottom plate does not translate to horizontal momentum across the layer to induce waves. Therefore, the fluidizing gas flow creates relatively uniform vertical motion and forces on particles across the layer such that particles collide nearly simultaneously with the bottom plate, allowing waves to form. In contrast, a lack of gas flow causes the particles to move differently at the top and bottom of the layer such that collisions occur at different times in different positions in the layer.

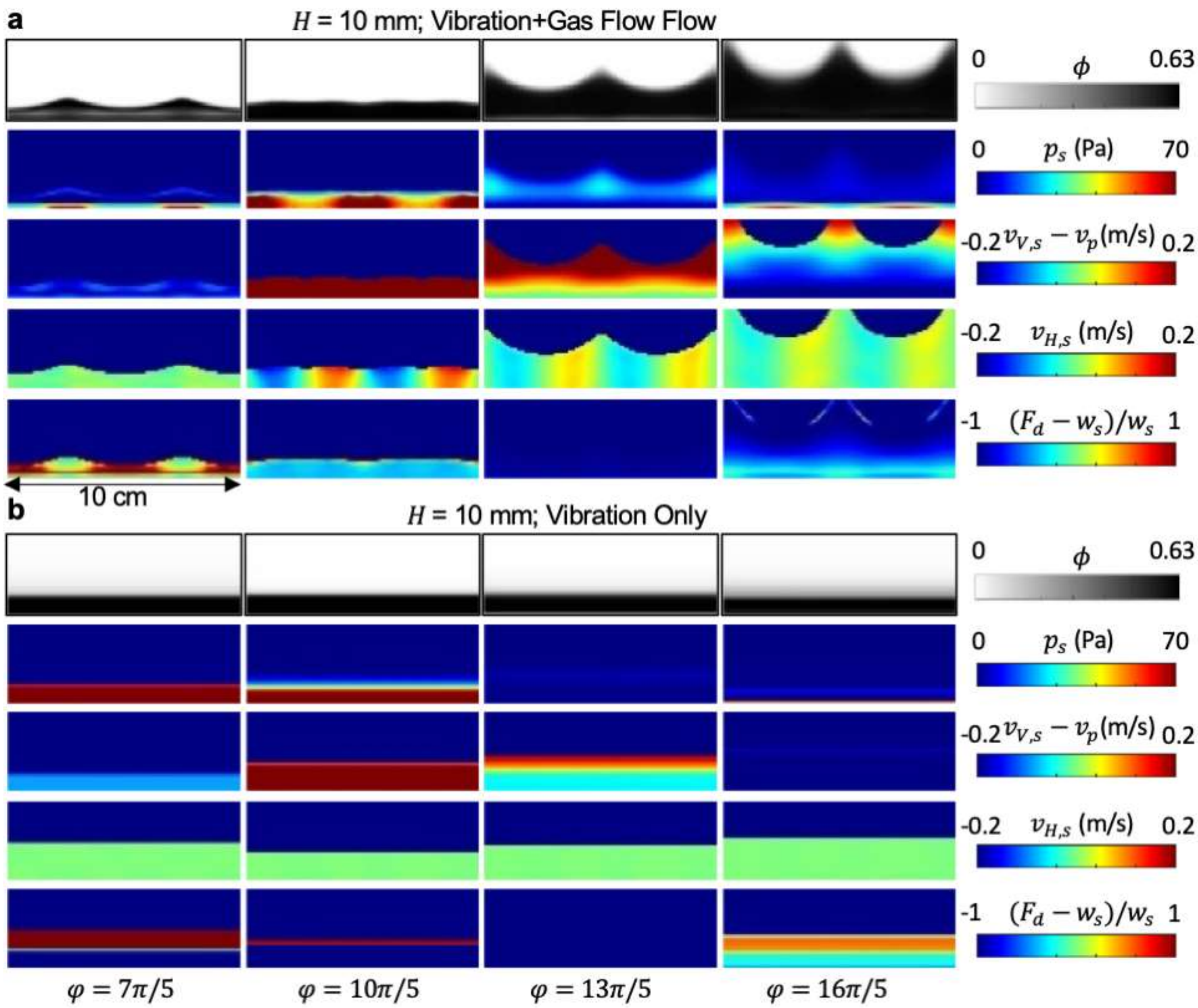

Fig. 6 Time series of vertical slice images from continuum simulations for the cases with H/d_p = 40 with and without constant gas flow from **Fig. 5**. Solids volume fraction (ϕ), solids pressure (p_s), vertical solids velocity relative to plate velocity ($v_{V,s} - v_p$), horizontal solids velocity ($v_{H,s}$) and normalized difference between drag force and solids weight ($(F_d - w_s)/w_s$) are shown.

IV. CONCLUSION

In conclusion, this work demonstrates that combined gas flow and vibration can induce Faraday wave patterns in granular particles, forming at lower vibration strengths and persisting at much taller layer heights than if vibration alone is used. The regimes formed depend on vibration conditions, gas flow conditions and layer height, and a parameter u_{tot}^* introduced here captures both vibration and gas flow effects to collapse data for the onset of waves when plotted against f^*. Continuum simulations utilizing a recently developed rheological model can capture wave patterns in granular particles. These simulations demonstrate that gas flow increases the uniformity of forces on particles in tall layers, allowing particles throughout the layer to move in more coordinated motion to form waves. Overall, the scalability and structured nature of the granular waves formed here enable potential industrial applications. Further, the bridging of behavior between Faraday waves in conventional fluids and vibrated grains and the ability to model these flows computationally using continuum models create pathways to investigate Faraday waves across a range of complex fluids.

Acknowledgment

This work was funded by National Science Foundation Award #2144763.

References:

[1] P. Richard, M. Nicodemi, R. Delannay, P. Ribière, and D. Bideau, *Slow Relaxation and Compaction of Granular Systems*, Nat. Mater. **4**, 2 (2005).
[2] M. Rauter, S. Viroulet, S. S. Gylfadóttir, W. Fellin, and F. Løvholt, *Granular Porous Landslide Tsunami Modelling – the 2014 Lake Askja Flank Collapse*, Nat. Commun. **13**, 1 (2022).
[3] H. Wang, A. Mustaffar, A. N. Phan, V. Zivkovic, D. Reay, R. Law, and K. Boodhoo, *A Review of Process Intensification Applied to Solids Handling*, Chem. Eng. Process. Process Intensif. **118**, 78 (2017).
[4] D. J. Goldfarb, B. J. Glasser, and T. Shinbrot, *Shear Instabilities in Granular Flows*, Nature **415**, 302 (2002).
[5] H. K. Pak and P. R. Behringer, *Bubbling in Vertically Vibrated Granular Materials*, Nature **371**, 231 (1994).
[6] J. F. Davidson and D. Harrison, *Fluidised Particles* (Cambridge University Press, Cambridge, 1963).
[7] R. D. Maladen, Y. Ding, C. Li, and D. I. Goldman, *Undulatory Swimming in Sand: Subsurface Locomotion of the Sandfish Lizard*, Science **325**, 314 (2009).
[8] U. D'Ortona and N. Thomas, *Self-Induced Rayleigh-Taylor Instability in Segregating Dry Granular Flows*, Phys. Rev. Lett. **124**, 178001 (2020).

[9] J. Duran, *Rayleigh-Taylor Instabilities in Thin Films of Tapped Powder*, Phys. Rev. Lett. **87**, 254301 (2001).
[10] C. P. McLaren, T. M. Kovar, A. Penn, C. R. Muller, and C. M. Boyce, *Gravitational Instabilities in Binary Granular Materials*, Proc. Natl. Acad. Sci. **116**, 9263 (2019).
[11] Q. Guo, Y. Zhang, T. M. Kovar, K. Xi, and C. M. Boyce, *A Rayleigh–Bénard Convection Instability Analog in Vibrated Gas-Fluidized Granular Particles*, Soft Matter **18**, 3323 (2022).
[12] Q. Guo, Y. Zhang, A. Padash, K. Xi, T. M. Kovar, and C. M. Boyce, *Dynamically Structured Bubbling in Vibrated Gas-Fluidized Granular Materials*, Proc. Natl. Acad. Sci. **118**, e2108647118 (2021).
[13] J. R. Royer, D. J. Evans, L. Oyarte, Q. Guo, E. Kapit, M. E. Möbius, S. R. Waitukaitis, and H. M. Jaeger, *High-Speed Tracking of Rupture and Clustering in Freely Falling Granular Streams*, Nature **459**, 1110 (2009).
[14] I. S. Aranson and L. S. Tsimring, *Patterns and Collective Behavior in Granular Media: Theoretical Concepts*, Rev. Mod. Phys. **78**, 641 (2006).
[15] M. O. Coppens and J. R. van Ommen, *Structuring Chaotic Fluidized Beds*, Chem. Eng. J. **96**, 117 (2003).
[16] C. S. Daw, C. E. A. Finney, M. Vasudevan, N. A. van Goor, K. Nguyen, D. D. Bruns, E. J. Kostelich, C. Grebogi, E. Ott, and J. A. Yorke, *Self-Organization and Chaos in a Fluidized Bed*, Phys. Rev. Lett. **75**, 2308 (1995).
[17] E. W. Merrow, *Linking R&D to Problems Experienced in Solids Processing*, (1984).
[18] J. Miles, *On Faraday Waves*, J. Fluid Mech. **248**, 671 (1993).
[19] F. Melo, P. Umbanhowar, and H. L. Swinney, *Transition to Parametric Wave Patterns in a Vertically Oscillated Granular Layer*, Phys. Rev. Lett. **72**, 172 (1994).
[20] P. B. Umbanhowar, F. Melo, and H. L. Swinney, *Localized Excitations in a Vertically Vibrated Granular Layer*, Nature **382**, 793 (1996).
[21] F. Melo, P. B. Umbanhowar, and H. L. Swinney, *Hexagons, Kinks, and Disorder in Oscillated Granular Layers*, Phys. Rev. Lett. **75**, 3838 (1995).
[22] C. Bizon, M. D. Shattuck, J. B. Swift, W. D. McCormick, and H. L. Swinney, *Patterns in 3D Vertically Oscillated Granular Layers: Simulation and Experiment*, Phys. Rev. Lett. **80**, 57 (1998).
[23] E. Cerda, F. Melo, and S. Rica, *Model for Subharmonic Waves in Granular Materials*, Phys. Rev. Lett. **79**, 4570 (1997).
[24] L. de Martín, C. Ottevanger, J. R. van Ommen, and M.-O. Coppens, *Universal Stability Curve for Pattern Formation in Pulsed Gas-Solid Fluidized Beds of Sandlike Particles*, Phys. Rev. Fluids **3**, 034303 (2018).
[25] J. Li, I. S. Aranson, W.-K. Kwok, and L. S. Tsimring, *Periodic and Disordered Structures in a Modulated Gas-Driven Granular Layer*, Phys. Rev. Lett. **90**, 134301 (2003).
[26] V. Francia, K. Wu, and M.-O. Coppens, *Dynamically Structured Fluidization: Oscillating the Gas Flow and Other Opportunities to Intensify Gas-Solid Fluidized Bed Operation*, Chem. Eng. Process. - Process Intensif. **159**, 108143 (2021).
[27] S. E. Lehmann, E.-U. Hartge, A. Jongsma, I.-M. deLeeuw, F. Innings, and S. Heinrich, *Fluidization Characteristics of Cohesive Powders in Vibrated Fluidized Bed Drying at Low Vibration Frequencies*, Powder Technol. **357**, 54 (2019).
[28] C. R. Wassgren, C. E. Brennen, and M. L. Hunt, *Vertical Vibration of a Deep Bed of Granular Material in a Container*, J. Appl. Mech. **63**, 712 (1996).

[29] J. C. Virnig, A. S. Berman, and P. R. Sethna, *On Three-Dimensional Nonlinear Subharmonic Resonant Surface Waves in a Fluid: Part II—Experiment*, J. Appl. Mech. **55**, 220 (1988).
[30] *See Supplemental Material at ****** for Supplemental Figures and Tables and a Movie Showing Optical Imaging Experiments as Well as Continuum Simulations of the Faraday Waves of Granular Particles Excited by Combined Constant Gas Flow and Vibration.*, (2023).
[31] C. P. McLaren, J. P. Metzger, C. M. Boyce, and C. R. Müller, *Reduction in Minimum Fluidization Velocity and Minimum Bubbling Velocity in Gas-Solid Fluidized Beds Due to Vibration*, Powder Technol. **382**, 566 (2021).
[32] J. Ding and D. Gidaspow, *A Bubbling Fluidization Model Using Kinetic Theory of Granular Flow*, AIChE J. **36**, 523 (1990).
[33] D. Gidaspow, *Multiphase Flow and Fluidization: Continuum and Kinetic Theory Descriptions* (Academic Press, 1994).
[34] J. M. Musser and J. E. Carney, Theoretical Review of the MFIX Fluid and Two-Fluid Models, No. DOE/NETL-2020/2100, NETL, 2020.
[35] C. K. K. Lun, S. B. Savage, D. J. Jeffrey, and N. Chepurniy, *Kinetic Theories for Granular Flow: Inelastic Particles in Couette Flow and Slightly Inelastic Particles in a General Flowfield*, J. Fluid Mech. **140**, 223 (1984).
[36] S. Ergun, *Fluid Flow through Packed Columns*, Chem. Eng. Prog. **48**, 89 (1952).
[37] A. Srivastava and S. Sundaresan, *Analysis of a Frictional–Kinetic Model for Gas–Particle Flow*, Powder Technol. **129**, 72 (2003).
[38] D. G. Schaeffer, *Instability in the Evolution Equations Describing Incompressible Granular Flow*, J. Differ. Equ. **66**, 19 (1987).